Asian Journal of Chemistry; Vol. 37, No. 12 (2025), 3116-3126
ASIAN JOURNAL OF CHEMISTRY
https://doi.org/10.14233/ajchem.2025.34753

Green Synthesis and Characterization of Ag/ZnO Bimetallic Nanocomposites Using *Evodia fraxinifolia* Fruit Extract: Evaluation of Photocatalytic, Antimicrobial and Antioxidant Activities

B.R. CHHETRI[1], S. JHA[1,*], N.K. BHATTACHARYYA[2,*], K.G. DOLMA[3] and A.M. DAS[4]

[1]Department of Chemistry, Sikkim Manipal Institute of Technology, Sikkim Manipal University, Majitar-737136, India
[2]Office of the Controller of Examination, Assam Women's University, Jorhat, Rowriah-785004, India
[3]Department of Microbiology, Sikkim Manipal Institute of Medical Sciences, Sikkim Manipal University, Tadong-737102, India
[4]Chemical Science and Technology Division, North East Institute of Science and Technology, Jorhat-785006, India

*Corresponding authors: E-mail: sangeeta.j@smit.smu.edu.in; nkamalbhatt@gmail.com

Received: 23 August 2025 *Accepted*: 30 October 2025 *Published online*: 30 November 2025 AJC-22203

The present work reports the green synthesis of Ag/ZnO nanocomposites (NCs) using *Evodia fraxinifolia* fruit extract, along with the evaluation of their photocatalytic, antimicrobial and antioxidant activities. The synthesized bimetallic NCs were characterized using X-ray diffraction (XRD), ATR-FTIR, UV-vis spectroscopy and scanning electron microscopy (SEM). FTIR confirmed the presence of secondary phytochemicals facilitating the synthesis of nanoparticles. XRD confirmed a crystalline nature with an average particle size of 27.9 nm. The SEM data confirmed the spherical shape of the nanoparticles and the distribution of the constituent elements was confirmed by elemental mapping. Photocatalytic studies revealed the 8% Ag/ZnO NCs exhibited the highest photocatalytic degradation efficiency for methylene blue (MB) and methyl orange (MO). Antibacterial test showed 8% Ag/ZnO NCs greater inhibition zone against *E. coli* (14 ± 0.6 mm) compared to *S. aureus* (10 ± 0.3 mm). The 8% Ag/ZnO demonstrated significant antioxidant activity of 61.13 % with IC_{50} value 71.6 µg/mL. Based on the obtained results, it is found that *E. fraxinifolia* fruit extract can be effectively employed in the synthesis of Ag/ZnO nanocomposites with material characterization and biological evaluations confirming their potential for biomedical applications.

Keywords: Green synthesis, *Evodia fraxinifolia*, Ag/ZnO Nanocomposites, Antimicrobial, Antioxidant, Photocatalytic.

INTRODUCTION

Photocatalytic conversion of organic pollutants into non-toxic products has become an important strategy for environmental remediation. Growing industrial activity has increased the release of pesticides, dyes, solvents and other contaminants, including carcinogenic intermediates such as aromatic azo dyes, which account for nearly half of global dye production. These are a major class of synthetic organic compounds known to cause hypersensitivity and allergies [1]. Various methods have been employed for the photocatalytic degradation of dyes, with varying degrees of success. Semiconductors are among the most researched and widely used materials, either in their pure form, with induced defects, as doped materials or in combination with other materials [2,3].

ZnO is recognized as a prominent photocatalyst and has garnered significant attention in the advancement of materials for the complete mineralization and degradation of environmental pollutants. This is attributed to its excellent photosensitivity, high physical and chemical stability, ease of synthesis, tunable morphology, cost-effectiveness and environmental compatibility [4]. However, pure ZnO has limitations, including a restricted absorption range (primarily UV), inefficient electron-hole separation and suboptimal redox potentials for photo-oxidative reactions [5]. Among metal nanoparticles, AgNPs are preferred because of their exceptional properties and high activity, contributing to the advancement in biosensors, agriculture, pharmaceuticals and water treatment [6]. Despite their enormous potential, AgNPs are less effective due to agglomeration caused by their high reactivity, strong inter-particle interaction and surface forces [5]. To maintain its effectiveness and prevent agglomeration, silver nanoparticles can be incorporated into semiconductor-based heterostructures like ZnO, to increase their efficiency and functionality [7]. The doping of AgNPs into the ZnO structure can prevent agglomeration and reduce particle size by reducing inter-particle attraction [8]. Shreema *et al.* [7] demonstrated that doping with pure ZnO reduced agglomeration and improved particle

separation. Furthermore, doping metallic elements into ZnO has found to increase its antimicrobial and antioxidant efficiency by improving electron-hole (e–h) separation, which in turn boosts its photocatalytic activity [9]. These nanoparticles demonstrate significant effectiveness against a range of antibiotic-resistant pathogenic bacteria.

Similarly, nanoparticles with antioxidant properties have garnered significant interest due to their potential to mitigate oxidative stress and their pivotal roles in nanoscience, nanotechnology and pharmaceutical sciences [10]. In addition, the chemical stabilizing agents like polyvinylpyrrolidone (PVP), polyacrylonitrile (PAN), hyperbranched polyurethane (HP) and polyvinyl alcohol (PVA) can be used to control the agglomeration of silver nanoparticles [11]. However, nanoparticles synthesized through chemical methods have been reported to release toxic substances at the nanoscale, potentially contributing to an increased risk of diseases such as cancer [12]. Consequently, chemically synthesized nanoparticles may pose a threat to environmental sustainability and restrict their applications in human consumption-related fields. Furthermore, the physical techniques used to prevent agglomeration, such as thermal ablation, milling and grinding have been associated with significantly low yields relative to the energy input [13]. To overcome these issues, green chemistry technology promotes substituting conventional chemicals with non-toxic and eco-friendly reducing agents [14]. In this approach, nanoparticles are synthesized using bioactive compounds derived from fungi, bacteria and plants which function as both reducing and stabilizing agents [15]. Among these sources, plant extracts are particularly used, as their composition and concentration of bioactive constituents significantly influence the characteristics of the resulting nanoparticles [16]. Plant extracts offer several advantages over conventional chemicals, including easy availability, biodegradability and minimal harmful effects. However, only a defined number of plant species have been scientifically validated for their effectiveness in green synthesis [17]. These plant species contain secondary phytochemicals such as alkaloids, polyphenols, tannins, proteins, terpenoids, flavonoids and saponins which function as reducing agents, converting metal ions into metal atoms [18]. Thus, green synthesis provides a foundation for developing non-toxic nanomaterials with potential applications in drug formulation and water treatment, ensuring minimal side effects [19].

Evodia fraxinifolia belongs to the Rutaceae family and it is extensively used as a traditional medicinal plant. Its fruits, roots and bark are used in treating gastrointestinal disorders like diarrhea, dysentery, indigestion and stomach ulcers, as well as conditions such as nausea, fever, skin diseases and abdominal pain. It has been used for birth control and vomiting treatment in traditional medicine [20]. Studies have reported the presence of secondary substances in significant amounts, such as phenols, tannins, terpenoids, saponins, amino acids, carbohydrates, steroids, alkaloids and flavonoids, which are crucial for green synthesis as stabilizing and reducing agents [21,22]. The current work reports the green synthesis of Ag/ZnO nanocomposites (NCs) using the fruit of *Evodia fraxinifolia*. Furthermore, the photocatalytic, antimicrobial and antioxidant activity of the synthesized nanoparticles was investigated to explore the potential of *E. fraxinifolia* fruit extract in the green synthesis of Ag/ZnO NCs using silver and zinc nitrates as precursors.

EXPERIMENTAL

The fruit of *Evodia fraxinifolia* was collected during summer from Uttarey, West Sikkim, India (88.0949ºS, 27.2605ºN) at an altitude of 2259 m. The voucher specimen was authenticated and deposited in Botanical Survey of India- SRH, Gangtok, Sikkim with accession no. BRC/15.

Methylene blue dye ($C_{16}H_{18}ClN_3S$), methyl orange dye ($C_{14}H_{14}N_3NaO_3S$), zinc nitrate hexahydrate ($Zn(NO_3)_2{\cdot}6H_2O$), silver nitrate ($AgNO_3$), sodium hydroxide (NaOH), ascorbic acid ($C_6H_8O_6$), used in this experiment were procured from Merck Ltd. India. 2,2-Diphenyl-1-picrylhydrazyl (DPPH), was procured from SLR Fine Chemicals Pvt. Lt., India and all the chemicals were used without any further purifications. All the analytical precursors were prepared using double-distilled water.

Preparation of *E. fraxinifolia* fruit extract: The collected fruits were dried in the shade at room temperature and crushed into fine powder. The powdered material was kept in a closed container for further use. In order to ensure adequate phytochemical extraction, 20 g of fruit powder were mixed with 100 mL of distilled water and subjected to magnetic stirring for 24 h. The subsequent extract was then centrifuged and filtered through Whatman paper to remove the fruit particles from the extract. The resultant extract was kept at 4 ºC and was used for the green synthesis of Ag/ZnO NCs.

Green synthesis of Ag/ZnO NCs: For the synthesis of Ag/ZnO nanocomposite, we have used the green synthesis approach as described in the literature with a slight modification [23]. In brief, $ZnNO_3$ (2.9748 g) was slowly added to 90 mL of *E. fraxinifolia* fruit extract under a magnetic stirrer for 30 min, followed by 10 mL of $AgNO_3$ solution (0.01 M) for another 30 min at 80 ºC, resulting in a final concentration of 1 mM $AgNO_3$ and 0.1 M $Zn(NO_3)_2{\cdot}6H_2O$. The pH initially dropped from 5 to 4, after which it was adjusted at 7-8 by the gradual addition of 0.1 M NaOH solution. The reaction was accompanied by a sequential colour change from brown color of fruit extract to pale yellow on addition of $Zn(NO_3)_2$, to dark yellow after addition of $AgNO_3$ solution, indicating the reduction of Ag^+ and Zn^+ ions and dark green when NaOH solution was added. After cooling to room temperature, the batches were washed with 50% ethanol and centrifuged at 4000 rpm. The precipitates were collected and oven-dried for 4 h at 80 ºC and then calcinated for 2 h at 450 ºC. The resultant nanohybrid crystals were ground into powder and used for characterization and activity tests. Following a similar procedure, four batches with different dopant concentrations of $AgNO_3$, corresponding to $[Ag^+]/[Zn^{2+}]$ molar ratio of 1%, 3%, 5% and 8% were synthesized, respectively.

Characterization: The synthesized Ag/ZnO NCs were analyzed by X-ray diffraction using Rigaku Ultima III with a Cu kα radiation source (λ = 1.5417 Å). The Attenuated Total Reflection-Fourier transform infrared (ATR-FTIR) spectroscopy (IRA-1S WL(ENG230V); Shimazu, Japan) was used for functional groups analysis with the spectral range of 4000-400 cm^{-1}. The ultraviolet-visible (UV-1900i Shimadzu, Japan)

dual beam spectrophotometer was used to study the optical properties of the nanoparticles, photocatalytic and antioxidant activities in the range of 200-800 nm. The morphology and elemental composition of nanomaterials were examined by field emission scanning electron microscopes (FE-SEM) coupled with energy dispersive X-ray spectroscopy (EDX).

Photocatalytic activity: For this activity, the synthesized Ag/ZnO NCs of 1%, 3%, 5% and 8% were used against a common organic pollutants; methylene blue (MB) as a cationic dye and methyl orange (MO) as an anionic dye in the presence of natural sunlight. In this activity, 50 mg of each sample of Ag/ZnO NCs was added to 50 mL of aqueous organic dye solution (10^{-5} M). Secondly, to achieve an adsorption-desorption condition between the catalyst and reactant, photocatalytic solutions were left in dark for 60 min under constant magnetic stirring. After the solutions were exposed to sunlight, a 4 mL suspension was taken from the solution mixture at 5 min intervals for a total duration of 30 min. The nanocatalyst was separated by centrifugation at 4000 rpm and the absorbance of the supernatant was recorded using a UV-Vis spectrophotometer at λ_{max} = 664 nm (MB) and λ_{max} = 464 nm (MO). Using the following equation, the percentage (%) photocatalytic degradation efficiency (D) was determined.

$$D\ (\%)\frac{C_c - C_s}{C_c} \times 100 \qquad (1)$$

where C_c and C_s are the initial and subsequent dye concentration at t (min), respectively.

Antioxidant activity: The antioxidant activity of the synthesized Ag/ZnO NCs was evaluated using 2,2-diphenyl-1-picrylhydrazyl (DPPH) assay. In this process, 1 mL of 0.1 mM methanolic DPPH and 3 mL of 8% Ag/ZnO sample at varying concentrations (20-100 μg mL^{-1}) were mixed. After 30 min of dark incubation, the optical density (O.D.) was measured at 517 nm on the wavelength. As a reference, ascorbic acid was utilized. The percentage scavenging activity was determined by following eqn. 2:

$$\text{DPPH radical scavenging}\ (\%) = \frac{A_o - A_s}{A_o} \times 100 \qquad (2)$$

where A_0 is control O.D. and A_S is O.D. of sample.

Antimicrobial activity: The synthesized Ag/ZnO NCs antimicrobial activity was determined against *Escherichia coli*, as Gram-negative bacteria, *Staphylococcus aureus* as Gram-positive bacteria and *Candida albicans* as fungal, using the well diffusion method. The microorganism was collected from the Microbiology Lab, Sikkim Manipal Institute of Medical Science, Gangtok, India. All the required glassware was sterilized using an autoclave process before starting the experiment to avoid the unconditional contamination. The tested cell suspensions were kept at 0.5 McFarland turbidity standards with an inoculum of 1×10^8 CFU mL^{-1}. The Mueller-Hinton agar and potato dextrose agar plates were coated with each bacterial and fungal suspension and the plates were left for 15 min to dry. The Ag/ZnO (1, 3, 5 and 8%) NCs at concentration of 50 mg/mL, with a dilution of 100 μL were loaded to 6 mm diameter wells punched on the agar plates. After incubating the plates for 24 h at 37 ºC, the zones of inhibition surrounding each well were measured.

RESULTS AND DISCUSSION

Structural and morphological analysis: Fig. 1 represents the X-ray diffraction patterns of the 8% Ag/ZnO NCs, which offers the crystallographic fingerprint of the materials. The diffraction peaks for ZnO correspond to the 2θ values of 31.8º, 34.4º, 36.2º, 47.6º, 56.5º, 62.7º, 67.8º, 72.6º, which are indexed to the crystal planes of (100), (002), (101), (102), (110), (103), (112) and (004) of hexagonal wurtzite structures of ZnO, respectively (JCPD card no. 36-1451) [24]. Moreover, the Ag/ZnO NCs show additional peaks on doping with the silver salts at 38.1º, 44.2º, 72.5º and 77.1º, which matches with (111), (200), (220) and (311) planes, respectively. The face center cubic (fcc) of Ag nanoparticles (JCPD card no. 04-0783) is indexed to these peaks, suggesting the presence of Ag nanoparticles in the composite [25]. The low intensity of the Ag peaks indicates the low concentration of silver nanoparticles. The average crystallite size of the Ag/ZnO NCs was defined using the Scherrer equation (eqn. 3) and was observed to be 27.9 nm:

$$D = \frac{K\lambda}{\beta}\cos\theta \qquad (3)$$

where D is the average crystallite size (nm); K is the Scherrer constant (0.9); λ denotes the specific wavelength of X-ray (0.154 nm); θ is diffraction Bragg's angle and β represents full width at half maxima.

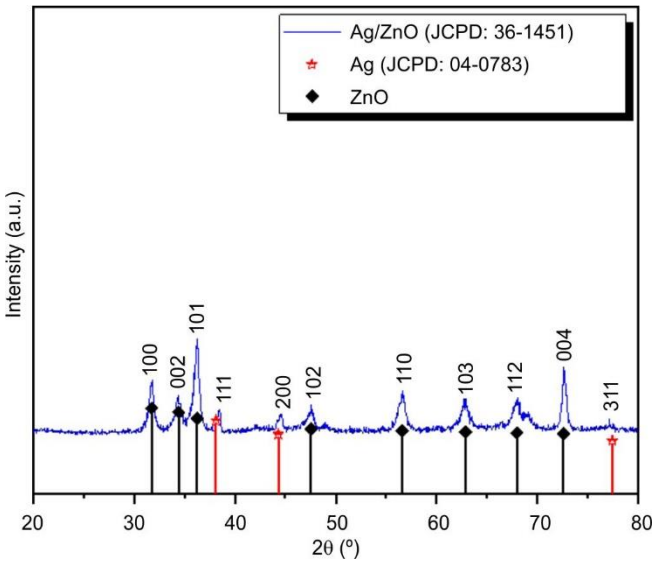

Fig. 1. XRD pattern of synthesized 8% Ag-ZnO nanocomposite using *E. fraxinifolia* fruit extract

ATR-FTIR spectral studies: The ATR-FTIR spectra of Ag/ZnO NCs with varying silver concentrations (1%, 3%, 5% and 8%) alongside the spectrum of *E. fraxinifolia* fruit extract, which acts as a stabilizing and reducing agent in the biosynthesis of nanomaterials is shown in Fig. 2. The peaks detected at 3333.7 cm^{-1}, 2952.9 cm^{-1}, 1729.7 cm^{-1} and 1025 cm^{-1} linked to O–H, C–H, C=O and C–N stretching, respectively. These peaks indicate the presence of bioactive compounds like flavonoids, tannins, alkaloids, reducing sugars and saponins alcohols, amides, polyphenols, esters and acids, suggesting the existence of alcohols, amides, polyphenols, esters

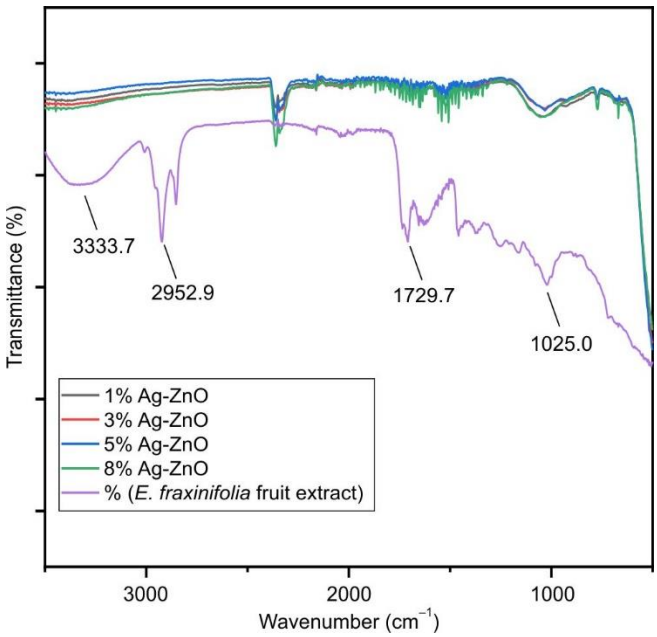

Fig. 2. FTIR spectra of Ag-ZnO NCs at different concentration and *Evodia fraxinifolia* plant extract

and acids [22]. After the formation of Ag-ZnO NCs, certain peaks attributed to *E. fraxinifolia* fruit extract (3333.7, 2952.9, 1729.7 and 1025 cm^{-1}) diminished, indicating the key role of phytochemicals in the stabilization and reduction of the nanomaterials. The broad peak at 3333.7 cm^{-1} signifies the presence of OH groups due to water adsorption on the nanoparticle surfaces [26]. Furthermore, the retention of the peak at 1025 cm^{-1}, associated with polyphenols from *E. fraxinifolia* extract, highlights the crucial role of these phytochemicals in preventing nanoparticle agglomeration by providing steric hindrance during synthesis [22]. These results provide strong evidence of the successful incorporation of bioactive molecules into Ag/ZnO nanocomposites *via* a green synthesis approach.

UV-visible studies: In this study, Ag/ZnO NCs were synthesized *via* a green method using an aqueous fruit extract of *E. fraxinifolia*. During the process, the fruit extract underwent a colour change from dark brown to pale yellow with the addition of $Zn(NO_3)_2$ and to dark yellow with silver nitrate addition. This serves as a primary confirmation of the formation of Ag and Zn nanoparticles in the solutions. The colour change arises from the activation of surface plasmon vibration in the AgNPs. Fig. 3 presents the UV-Vis absorption spectra of Ag-doped ZnO nanocomposites with varying silver concentrations (1%, 3%, 5% and 8%). The spectra reveal a gradual increase in absorbance with increasing silver content, emphasizing the increased light absorption due to the surface plasmon resonance (SPR) effect of AgNPs. Distinct absorption peaks are observed around 400-450 nm, corresponding to the distinctive SPR band of AgNPs, suggesting successful doping of Ag into the ZnO matrix [27]. The absorbance intensity follows the order: 8% Ag/ZnO > 5% Ag/ZnO > 3% Ag/ZnO > 1% Ag/ZnO, demonstrating a direct correlation between Ag concentration and optical absorption. The redshift in the absorption band with increasing Ag content suggests a bandgap energy reduction, due to the impurity energy levels introduction by Ag ions, which facilitates electron transitions. This phenomenon

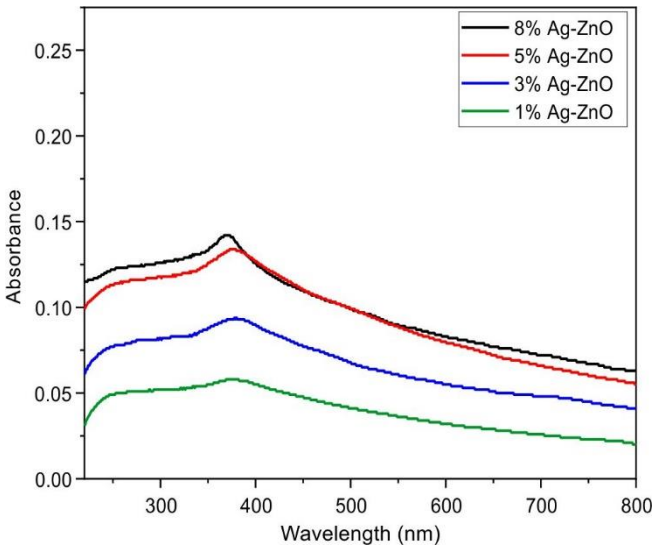

Fig. 3. UV-vis spectra of 1, 3, 5 and 8% Ag/ZnO NCs

further confirms the successful doping of silver into the zinc oxide structure, enhancing its optical properties.

Morphological studies: The morphological study (shape and size) of the synthesized Ag/ZnO NCs using *E. fraxinifolia* fruit extract was done using electron microscopy techniques such as SEM. Fig. 4a-b represents the SEM images of both low and high magnification of Ag/ZnO demonstrating spherical agglomerated composites. EDS spectra in Fig. 4c further demonstrate the existence of silver, zinc and oxygen in the Ag/ZnO NCs. This proved that fruit extract of *E. fraxinifolia* can be effectively utilized for the synthesis of Ag/ZnO NCs. The elemental composition in the nanocomposite exhibited peak of weight percentages 30.6%, 67.7% and 1.7% for oxygen, zinc and silver, respectively, while the atomic percentage of 64.5%, 35% and 0.5% for oxygen, zinc and silver, respectively. For zinc, the observed peak was around 8.8 keV, for oxygen strong peak at around 0.5 keV and for silver peak at around 3 keV, compliance with those reported by Honsy *et al.* [28]. The successful incorporation of silver into zinc oxide is confirmed by the EDAX mapping (Fig. 4d-f), which shows a consistent dispersion of silver, zinc and oxygen within the composite material. These findings strongly indicate the efficient incorporation of Ag^+ ions into the ZnO nanoparticles.

Photocatalytic activity: The photocatalytic activity of the synthesized Ag/ZnO NCs was conducted to measure the efficiency of the water-soluble MB and MO dyes under sunlight, which are extensively used in industrial sectors such as pharmaceuticals, textile, leather and printing. The Ag/ZnO NCs catalyzed of MB and MO dye degradation were monitored using a UV-vis spectrophotometer. It is demonstrated in Figs. 5a-d and 6a-d that with illumination time there is a decrease in the absorption peak of the MO and MB dye solutions. In both dye degradations, 8% Ag-ZnO nanocomposite showed the maximal reduction in absorption peak with the irradiation for about 30 min compared to the 1%, 3% and 5% nanocomposites. This observation aligns with the Beer-Lambert's law thereby confirming the reduction of dye concentration over time. To further quantify the photocatalytic kinetics, the relative concentration (C/C_o) of MB and MO dyes was accomplished. Fig. 7a-b depict the relative concentration (C/C_o) of MB and

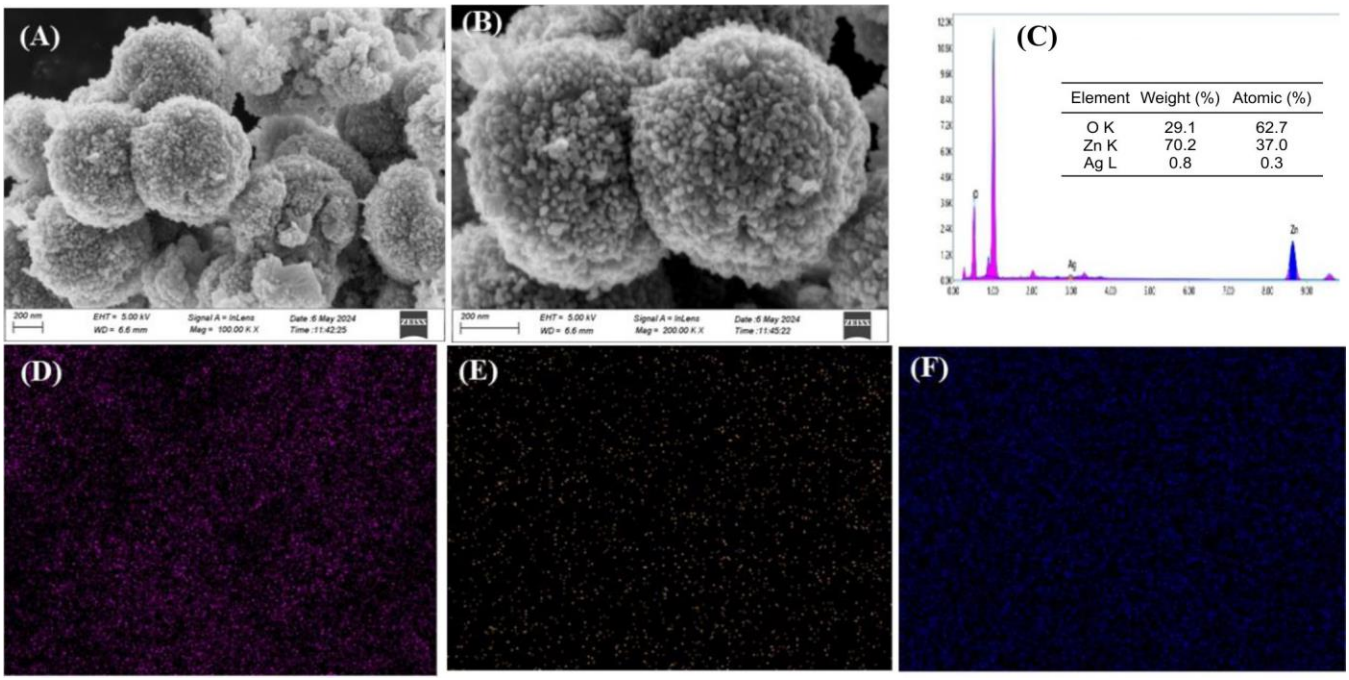

Fig. 4. SEM images of 8% Ag-ZnO at (a) low magnification, (b) high magnification, (c) EDX spectrum and elemental mapping results of (d) O, (e) Ag and (f) Zn elements of Ag/ZnO NCs synthesized using fruit extract of *E. fraxinifolia*

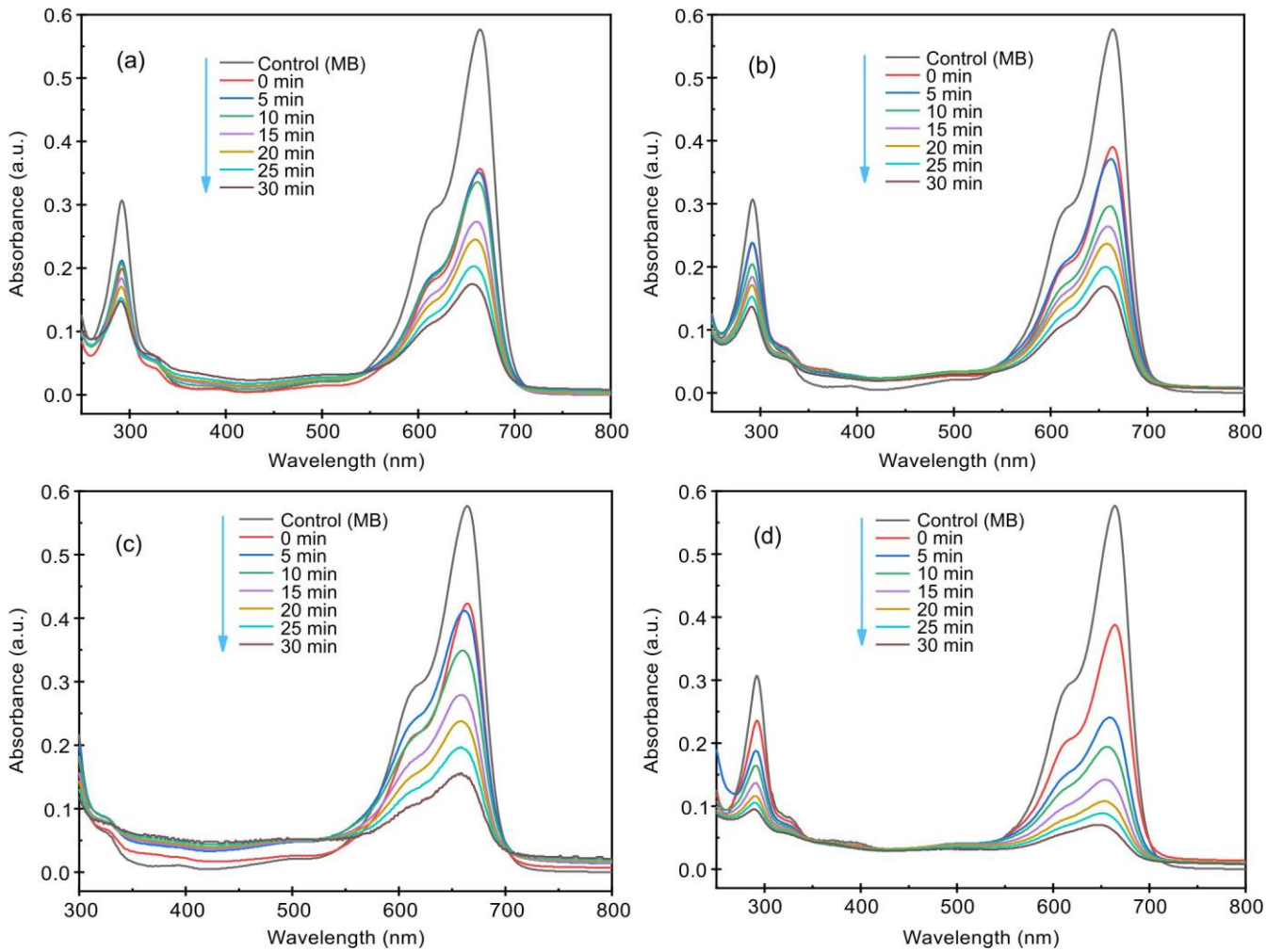

Fig. 5. UV-vis spectra for photodegradation of methylene blue in the presence of (a) 1%, (b) 3%, (c) 5%, and (d) 8% silver-zinc oxide NCs

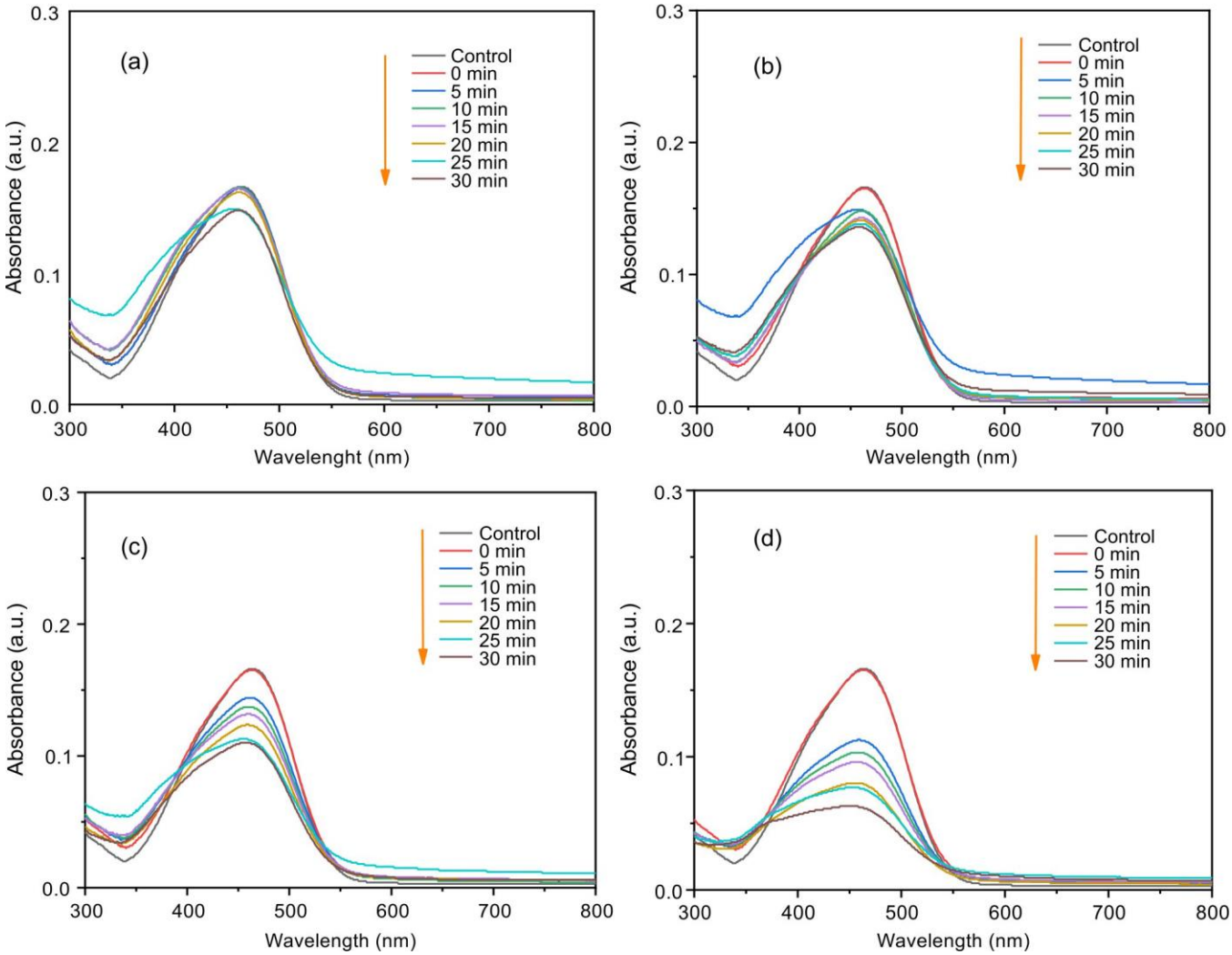

Fig. 6. UV-vis spectra for photodegradation of methyl orange in the presence of (a) 1%, (b) 3%, (c) 5% and (d) 8% silver-zinc oxide NCs

MO dyes as a function of irradiation time (t) for Ag/ZnO NCs, where C represents the dye concentration at irradiation time and C_o represents the dye concentration before irradiation. Before irradiation, the samples were subjected to a 60 min dark for adsorption/desorption equilibration period where only minimal reduction in dye concentration was detected, which indicates that the adsorption of MB and MO dyes on the samples is defined after the adsorption-desorption equilibrium is reached. Significantly, 8% Ag/ZnO nanocomposite demonstrated the most significant degradation within 30 min, surpassing 1%, 3% and 5% Ag/ZnO nanocomposites. To elucidate the influence of silver concentration within the ZnO matrix on photocatalytic reaction kinetics, the kinetic behaviour of the Ag-ZnO nanocomposites was determined. The rate equation, $\ln(C_o/C) = kt$, was employed to determine the reaction rate constant (k), where C_o and C represent the initial and time-dependent concentrations of MB and MO, respectively and t is the reaction time.

The calculated rate constants (k) for MB degradation were found to be 2×10^{-2} min, 3×10^{-2} min, 3.5×10^{-2} min and 6×10^{-2} min, respectively. For MO degradation, the corresponding k values were 0.4×10^{-2} min, 0.5×10^{-2} min, 1.2×10^{-2} min and 2.8×10^{-2} min for 1%, 3%, 5% and 8% Ag/ZnO NCs, respectively. Fig. 7c-d illustrates the relation between reaction rate (k) and Ag content in ZnO, where 8% Ag-ZnO nanocomposite exhibited the highest k value indicating enhanced photocatalytic activity, respectively. Further, Fig. 8a-b shows the percentage of MB and MO dyes degradation as a function of Ag concentration, demonstrating a direct correlation between Ag content and degradation efficiency. Specifically, the 8% Ag-ZnO nanocomposite achieved approximately 90% MB degradation and 63% MO degradation within 30 min of irradiation, significantly outperforming the 1%, 3% and 5% nanocomposites, which exhibited lower degradation efficiencies. These findings unequivocally establish the superior photocatalytic activity of the 8% Ag-ZnO NCs relative to the other compositions studied and the values are provided in Table-1.

Photocatalytic mechanisms: When the Ag/ZnO NCs are exposed to the sunlight with energy equal to or greater than its band gap, photoexcitation occurs, causing the excitation of electrons from the valence band (VB) to the conduction band (CB). This process generates electron-hole pairs, characterized by the formation of electron-deficient holes in the VB and electron-rich in the CB. Subsequently, the electrons in CB react with adsorbed molecular oxygen (O_2) to produce $^{\bullet}O_2^-$ radicals, while the hole in the VB reacts with H_2O

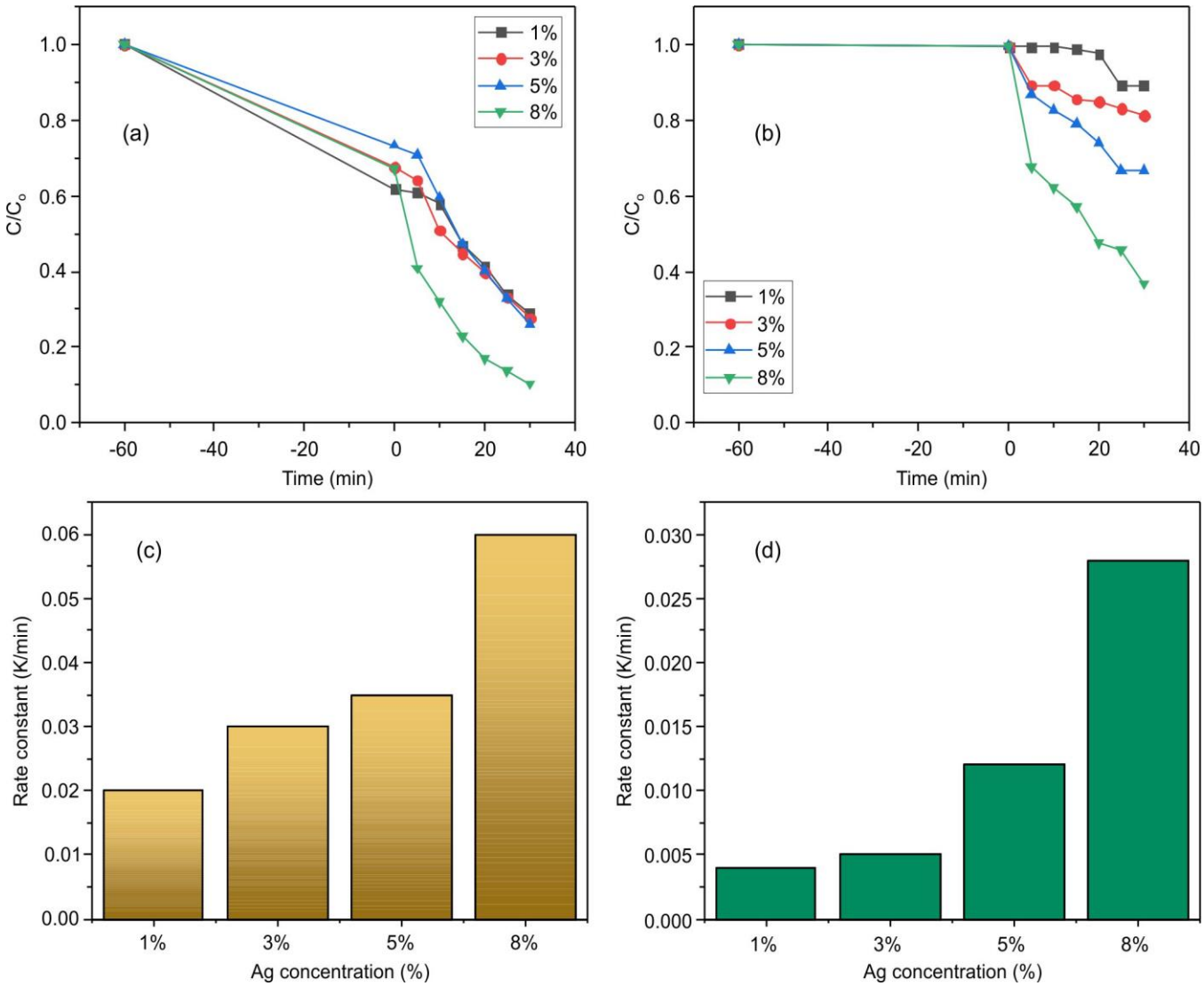

Fig. 7. C/C$_o$ *vs.* time (min) plot for the photodegradation of (a) MB and (b) MO; plot of rate constant *vs.* Ag concentration of (c) MB and (d) MO

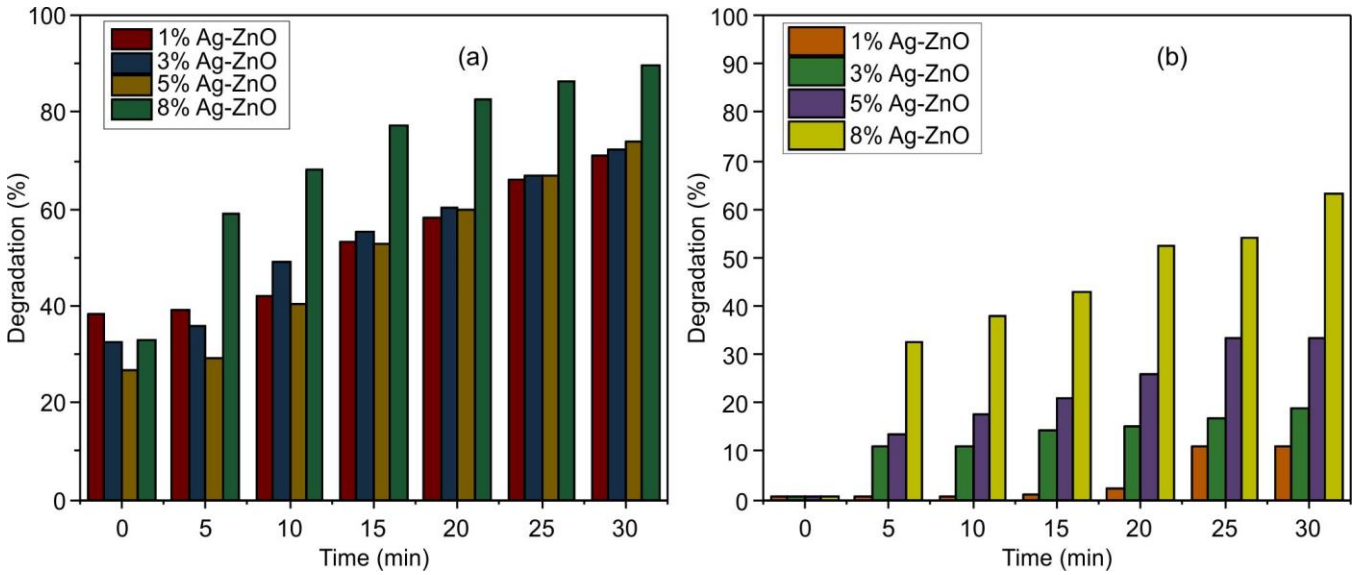

Fig. 8. Percentage dye degradation of (a) methylene blue (b) methyl orange

TABLE-1
PHOTOCATALYTIC PROPERTY COMPARISON OF Ag/ZnO NCs OVER MB AND MO DYES WITH THE LITERATURE

Material	Dye	Light source	Dye (mg/L)	Catalyst (mg)	Degradation time (min)	Dye degradation (%)	Ref.
Ag-ZnO	MB	Sunlight	5	10	80	96	[42]
Ag-ZnO	MB	Sunlight	5	10	120	80	[23]
Ag-ZnO	MB	Sunlight	1	10	120	94.27	[43]
Ag-ZnO	MB	Visible light	20	400	90	45	[44]
ZnO/Ag	MB & MO	Ultraviolet A	10	40	120 & 150	94 & 81	[45]
Ag-ZnO	MO & RhB	Xe lamp	10	40	35	99.7 & 99.3	[46]
Ag/ZnO	MB, MO & RhB	Sunlight	100	40	30	50, 68 & 72	[47]
Ag-ZnO	MB & MO	Sunlight	1	50	30	90 & 63	This work

molecules to generate OH^- radicals. These reactive oxygen species (ROS), characterized by their high reactivity and strong oxidizing potential, interact with the S atom of the C-S^+=C group, reducing C=N bond which facilitates demethylation processes, CO_2, H_2O and corresponding mineral acids in MB dye. On the other hand, the photocatalytic breakdown of MO dye molecules occurs by the N=N bond breaking down, causing the separation of the molecules [29]. The radicals then attack the CH_3–N–CH_3 group, which breaks down the –CH_3 group. One of the aromatic rings is then liberated and a sequence of intermediate reactions leads to the final byproducts of CO_2 and H_2O [30]. The presence of AgNPs anchored on the zinc oxide surface is posited to increase the formation rate of both $^{\bullet}O_2^-$ and $^{\bullet}OH$ radicals, thereby augmenting the degradation efficiency of organic pollutants. In present study, the percentage of MB dye degradation was higher than that of MO dye, which may be due to the simple aromatic structure of MB molecule making it more sensitive to ROS than the more complicated azo (-N=N-) structure of MO. Based on previous findings, the following equation explains the possible photocatalytic mechanism [31].

$$Ag-ZnO + h\nu \rightarrow Ag-ZnO\ (h^+ + e^-) \quad (4)$$

$$H^+ + OH^- \rightarrow H_2O \quad (5)$$

$$h^+ + OH^- \rightarrow OH^{\bullet}$$

$$e^- + O_2 \rightarrow O_2^{\bullet-} \quad (6)$$

$$H_2O + O_2^{\bullet-} \rightarrow OOH^- + OH^- \quad (7)$$

$$2OOH^{\bullet} \rightarrow O_2 + H_2O_2 \quad (8)$$

$$OH^{\bullet} + O_2^{\bullet-} + h_{vb}^+ + \text{Pollutants} \rightarrow \text{Degrade pollutants} \quad (9)$$

$$OH^{\bullet} + O_2^{\bullet-} + h_{vb}^+ + \text{Degrade pollutants} \rightarrow CO_2\uparrow + H_2O \quad (10)$$

Antimicrobial activity: The inhibitory properties of silver and zinc oxide nanoparticles have been widely used in a variety of medicinal applications, such as the inhibition of Gram-positive and Gram-negative bacterial strains [32]. A well-diffusion method was employed to investigate the antimicrobial efficiency of the synthesized Ag/ZnO against *S. aureus*, *E. coli* bacteria and *C. albicans*. The antimicrobial functioning of the nanoparticles follows two stages; first, they engage with the thiol groups in proteins to cause inactivation and then they interact with the DNA of the bacteria to condense the DNA and prevent DNA replication, which results in apoptosis [33]. Fig. 9 shows the inhibition zone for gentamycin and fluconazole marked as (+)ve control, 10% DMSO marked as (-)ve control and the synthesized 1%, 3%, 5% and 8% Ag/ZnO NCs, respectively. The gentamycin showed a ZOI of 20 ± 0.2 and 22 ± 0.4 mm for *S. aureus* and *E. coli*, respectively and fluconazole showed a ZOI of 25 ± 0.31 against *C. albicans*. As determined in Fig. 10, 8% Ag/ZnO NCs have confirmed the highest inhibition zone of 10 ± 0.3 and 14 ± 0.6 mm for both *S. aureus* and *E. coli* strains among the other synthesized NCs as reported else-where [34]. This viewpoint is impacted by the characteristics of both the nanoparticles as well as the bacterial cell wall and membrane

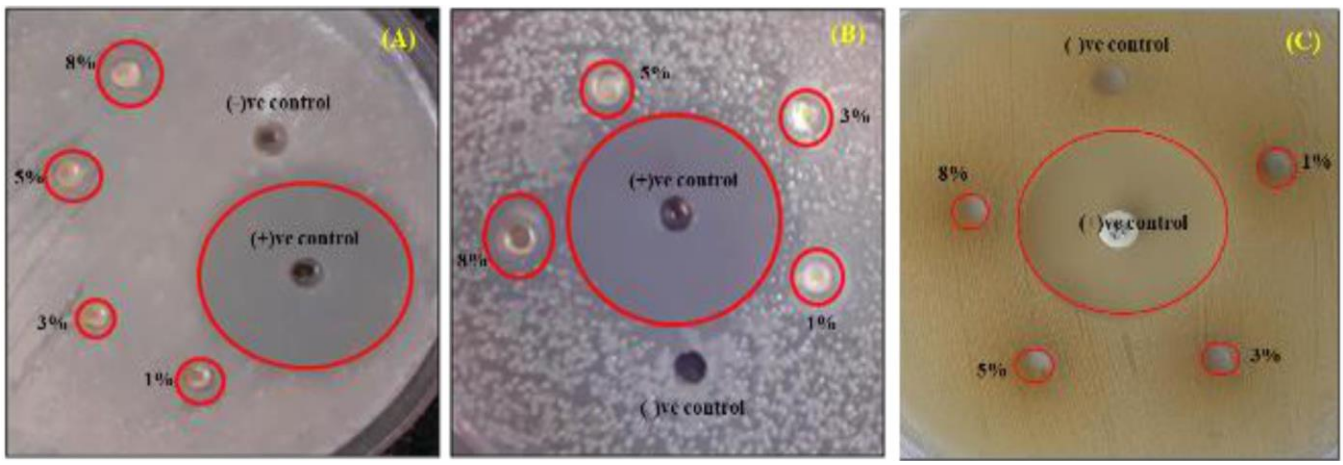

Fig. 10. Antimicrobial activity (zone of inhibition) of (1, 3, 5 and 8%) Ag-ZnO NCs nanocomposite against *S. aureus* (a), *E. coli* (b) and *C. albicans* (c)

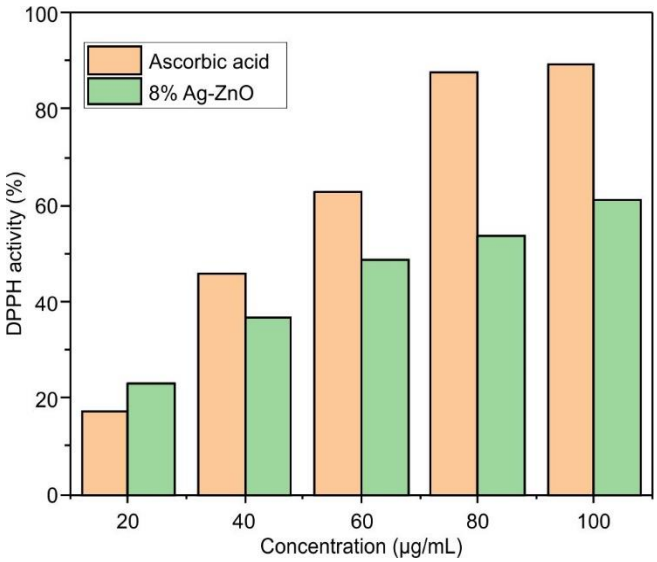

Fig. 9. Percentage scavenging of DPPH by 8% Ag-ZnO

properties. The peptidoglycan layer of Gram-positive bacteria is thick and hard, crosslinked by peptide chains, while that of Gram-negative bacteria is thin. Nanoparticles can more easily enter Gram-negative bacteria's nuclei due to their thin peptidoglycan coating, which prevents cell regeneration [26]. Also, the electrostatic interaction between positively charged nanoparticles and Gram-negative bacteria's negatively charged membrane enhances the efficiency of the nanoparticles to enter the bacterial cell, which is less effective in Gram-positive bacteria [35]. The Ag/ZnO NCs did not show any inhibition zone against *C. albicans*, which could be attributed to the inherent resistance mechanism of *C. albicans*, such as biofilm formation, adaptive tolerance and protective extracellular matrix which may hinder the effectiveness of these agents [36,37]. These findings are in good agreement with the previously reported studies and the values are reported in Table-2.

Antioxidant activity: The antioxidant capacity of the synthesized 8% Ag-ZnO nanocomposite was assessed using DPPH radical scavenging activity. It is a common and harmful free radical that poses risks to human health. The observed antioxidant activity of the 8% Ag-ZnO is likely due to its ability to donate electrons. This electron donation, from the nanocomposite's oxygen atoms to the unpaired electron of the DPPH nitrogen, diminishes the intensity of the n→π* transition at 517 nm, leading to the characteristic violet colour of DPPH fading to colourless [38]. The 8% Ag-ZnO nanocomposite showed a significant increase in DPPH scavenging activity, rising from 22.79% to 61.13% as its concentration increased from 20 to 100 µg/mL. In comparison, standard ascorbic acid exhibited even higher scavenging activity, ranging from 17.35% to 89.37% over the same concentration range (Fig. 10). These results are consistent with effective antioxidant activity and comparable to other reported studies where, RGO-ZnO nanocomposite showed 45% antioxidant efficiency, while another achieved only 14.85% DPPH scavenging [39]. The 8% Ag-ZnO nanocomposite showed IC_{50} value of 71.6 µg/mL, indicating its ability to inhibit 50% of DPPH radicals, while ascorbic acid, a standard antioxidant, showed a lower IC_{50} of 48.6 µg/mL, demonstrating higher potency. The antioxidant characteristics of metallic nanoparticles may be influenced by their chemical composition, concentration, elemental makeup and the inherent properties of the metal present [40]. Therefore, the antioxidant properties of Ag/ZnO NPs can be used in biomedical applications [41], enhancing packaged food shelf-life and other pertinent fields.

Conclusion

A straightforward, eco-friendly method, utilizing the fruit extract of *Evodia fraxinifolia*, was successfully employed to synthesize Ag/ZnO nanocomposites. This cost-effective and non-toxic approach, requiring only temperature and pH adjustments, avoided the need for external reagents or additives. XRD confirmed the crystalline structure of the synthesized Ag/ZnO nanoparticles, while FTIR identified the functional groups associated with the biomolecules present in the *E. fraxinifolia* fruit. The fruit extract served as a reducing/capping agent for AgNPs and facilitated the fabrication of ZnO and its composite with silver. EDX recorded the elemental composition of Ag/ZnO nanocomposites. The size of the resulting

TABLE-2
COMPARISON OF ANTIMICROBIAL ACTIVITY OF Ag/ZnO NCs OF THIS STUDY WITH OTHER STUDIES

Plant extract	Bacteria/fungus	Nanoparticles	Crystallite size (nm)	Zone of inhibition (nm)	Ref.
Launaea cornuta leaf extract	*Staphylococcus aureus* *Escherichia coli*	Ag/ZnO	21.51	15.5 ± 0.56 16.5 ± 0.46	[48]
Trigonella foenum-graecum leaf extract	*Staphylococcus aureus* *Escherichia coli*	Ag/ZnO	54	13.5 ± 0.707 12.5 ± 0.707	[49]
Pistacia atlantica resin	*Staphylococcus aureus* *Escherichia coli*	Ag/ZnO	18.9	12 ± 0.06 15.2 ± 0.007	[50]
Urginea epigea bulbs extract	*Staphylococcus aureus* *Escherichia coli*	Ag/ZnO	25.16	13 ± 0.3 19 ± 0.7	[51]
V. speciosum	*Staphylococcus aureus* *Escherichia coli*	Ag/ZnO	28.7	8.6 9.3	[22]
Tamarindus indica pulp extract	*Staphylococcus aureus* *Escherichia coli*	Ag/ZnO	38	19 ± 0.45 16 ± 0.49	[45]
Evodia fraxinifolia fruit extract	*Staphylococcus aureus* *Escherichia coli* *Candida albicans*	(1%, 3%, 5%, 8%) Ag/ZnO	36.11	6 ± 0.4, 4± 0.2, 8 ± 0.49, 10 ± 0.3 5 ± 0.8, 8 ± 0.4, 10 ± 0.2, 14 ± 0.6 Resistance	This work

nanocomposites played a role in their antibacterial effectiveness, with the addition of silver enhancing the antibacterial, antioxidant and photocatalytic properties of ZnO. The photocatalytic dye degradation experiments demonstrated that Ag/ZnO effectively breaks down both methylene blue and methyl orange dyes. After 30 min of irradiation, 8% Ag/ZnO achieved 90% and 61% degradation of the MB and MO dye mixture. These high degradation percentages, observed for both dyes, highlight the significant potential of Ag/ZnO as a highly efficient photocatalyst for the degradation of various hazardous dyes. The antioxidant potential of 8% Ag/ZnO may have been boosted by the alkaloids and phenolic compounds found in *E. fraxinifolia*. Moreover, 8% Ag/ZnO demonstrated substantial antibacterial activity against *S. aureus* and *E. coli*. This biogenic synthesis offers a viable route for producing nanoparticles for biological applications and the method could be adapted for creating other metal oxide nanoparticles, offering a more efficient alternative to traditional physical and chemical synthesis routes.

ACKNOWLEDGEMENTS

The authors are grateful to the Department of Chemistry, Sikkim Manipal Institute of Technology, Sikkim Manipal University for their great assistance. The authors also acknowledge the TMA Pai research grant for financial support to this research project work.

CONFLICT OF INTEREST

The authors declare that there is no conflict of interests regarding the publication of this article.

REFERENCES

1. B.A. Fahimmunisha, R. Ishwarya, M.S. AlSalhi, S. Devanesan, M. Govindarajan and B. Vaseeharan, *J. Drug Deliv. Sci. Technol.*, **55**, 101465 (2020); https://doi.org/10.1016/j.jddst.2019.101465
2. A. Balapure, J.R. Dutta and R. Ganesan, *RSC Appl. Interfaces*, **1**, 43 (2024); https://doi.org/10.1039/D3LF00126A
3. E. Kusmierek, *Catalysts*, **10**, 439 (2020); https://doi.org/10.3390/catal10040439
4. K.M. Lee, C.W. Lai, K.S. Ngai and J.C. Juan, *Water Res.*, **88**, 428 (2016); https://doi.org/10.1016/j.watres.2015.09.045
5. S. Pirtarighat, M. Ghannadnia and S. Baghshahi, *J. Nanostruct. Chem*, **9**, 1 (2019); https://doi.org/10.1007/s40097-018-0291-4
6. Z.A. Ratan, M.F. Haidere, M. Nurunnabi, S.M. Shahriar, A.J.S. Ahammad, Y.Y. Shim, M.J.T. Reaney and J.Y. Cho, *Cancers*, **12**, 855 (2020); https://doi.org/10.3390/cancers12040855
7. K. Shreema, R. Mathammal, V. Kalaiselvi, S. Vijayakumar, K. Selvakumar and K. Senthil, *Mater. Today Proc.*, **47**, 2126 (2021); https://doi.org/10.1016/j.matpr.2021.04.627
8. T.K.M. Prashantha Kumar, T.R. Mandlimath, P. Sangeetha, P. Sakthivel, S.K. Revathi, S.K. Ashok Kumar and S.K. Sahoo, *RSC Adv.*, **5**, 108034 (2015); https://doi.org/10.1039/C5RA19945J
9. M. Moradi, M. Haghighi and S. Allahyari, *Process Saf. Environ. Prot.*, **107**, 414 (2017); https://doi.org/10.1016/j.psep.2017.03.010
10. S.H. Nile, V. Baskar, D. Selvaraj, A. Nile, J. Xiao and G. Kai, *Nano-Micro Lett.*, **12**, 45 (2020); https://doi.org/10.1007/s40820-020-0383-9
11. V.K. Sharma, R.A. Yngard and Y. Lin, *Adv. Colloid Interface Sci.*, **145**, 83 (2009); https://doi.org/10.1016/j.cis.2008.09.002
12. M.M.I. Masum, M.M. Siddiqa, K.A. Ali, Y. Zhang, Y. Abdallah, E. Ibrahim, W. Qiu, C. Yan and B. Li, *Front. Microbiol.*, **10**, 820 (2019); https://doi.org/10.3389/fmicb.2019.00820
13. Priya, Naveen, K. Kaur and A.K. Sidhu, *Front. Nanotechnol.*, **3**, 655062 (2021); https://doi.org/10.3389/fnano.2021.655062
14. M.M.H. Khalil, E.H. Ismail, K.Z. El-Baghdady and D. Mohamed, *Arab. J. Chem.*, **7**, 1131 (2014); https://doi.org/10.1016/j.arabjc.2013.04.007
15. B. Mortezagholi, E. Movahed, A. Fathi, M. Soleimani, A. Forutan Mirhosseini, N. Zeini, M. Khatami, M. Naderifar, B. Abedi Kiasari and M. Zareanshahraki., *Microsc. Res. Tech.*, **85**, 3553 (2022); https://doi.org/10.1002/jemt.24207
16. V. Ramesh, K. Karthik, R. Cep and M. Elangovan, *Polymers*, **15**, 985 (2023); https://doi.org/10.3390/polym15040985
17. S. Ahmad, S. Munir, N. Zeb, A. Ullah, B. Khan, J. Ali, M. Bilal, M. Omer, M. Alamzeb, S.M. Salman and S. Ali., *Int. J. Nanomedicine*, **14**, 5087 (2019); https://doi.org/10.2147/IJN.S200254
18. A. Indriyani, Y. Yulizar, R.T. Yunarti, D.O.B. Apriandanu and R.M. Surya, *Appl. Surf. Sci.*, **563**, 150113 (2021); https://doi.org/10.1016/j.apsusc.2021.150113
19. S. Jadoun, R. Arif, N.K. Jangid and R.K. Meena, *Environ. Chem. Lett.*, **19**, 355 (2021); https://doi.org/10.1007/s10311-020-01074-x
20. R. Chanda, J. Mohanty, N. Bhuyan, P. Kar and L. Nath, *Indian J. Tradit. Knowl.*, **6**, 606 (2007).
21. Y.-X. Jiang, J.-Y. Yao, N. Qin, J.-J. Tan, F. Han, S.-J. Qu, S.-J. He and C.-H. Tan, *Fitoterapia*, **169**, 105606 (2023); https://doi.org/10.1016/j.fitote.2023.105606
22. B.R. Chhetri, N.K. Bhattacharyya, D. Dutta and K. Dolma, *Bioscene*, **21**, 1312 (2024).
23. N. Bala, S. Saha, P. Chakraborty, M. Maiti, M. Das, S.K. Basu, A. Nandy and S. Das, *RSC Adv.*, **5**, 4993 (2015); https://doi.org/10.1039/C4RA12784F
24. F. Ahmed, N. Arshi, M.S. Anwar, R. Danish and B.H. Koo, *RSC Adv.*, **4**, 24088 (2014); https://doi.org/10.1039/C4RA02470B
25. D.J. Binks and R.W. Grimes, *J. Am. Ceram. Soc.*, **76**, 2370 (1993); https://doi.org/10.1111/j.1151-2916.1993.tb07779.x
26. S.M. Mousavi-Kouhi, A. Beyk-Khormizi, M.S. Amiri, M. Mashreghi and M.E. Taghavizadeh Yazdi, *Ceram. Int.*, **47**, 21490 (2021); https://doi.org/10.1016/j.ceramint.2021.04.160
27. K.R. Basavalingiah, S. Harishkumar, G. Udayabhanu, G. Nagaraju, D. Rangappa and Chikkahanumantharayappa, *SN Appl. Sci.*, **1**, 935 (2019); https://doi.org/10.1007/s42452-019-0863-z
28. M. Hosny, M. Fawzy and A.S. Eltaweil, *Sci. Rep.*, **12**, 7316 (2022); https://doi.org/10.1038/s41598-022-11014-0
29. M.A. Abu-Dalo, S.A. Al-Rosan and B.A. Albiss, *Polymers*, **13**, 3451 (2021); https://doi.org/10.3390/polym13193451
30. P.A. Luque, H.E. Garrafa-Gálvez, O. Nava, A. Olivas, M.E. Martínez-Rosas, A.R. Vilchis-Nestor, A. Villegas-Fuentes and M.J. Chinchillas-Chinchillas, *Ceram. Int.*, **47**, 23861 (2021); https://doi.org/10.1016/j.ceramint.2021.05.094
31. N. Siva, D. Sakthi, S. Ragupathy, V. Arun and N. Kannadasan, *Mater. Sci. Eng. B*, **253**, 114497 (2020); https://doi.org/10.1016/j.mseb.2020.114497
32. S. Sudarsan, M. Kumar Shankar, A. Kumar Belagal Motatis, S. Shankar, D. Krishnappa, C.D. Mohan, K.S. Rangappa, V.K. Gupta and C.N. Siddaiah, *Biomolecules*, **11**, 259 (2021); https://doi.org/10.3390/biom11020259
33. S. Lokina, A. Stephen, V. Kaviyarasan, C. Arulvasu and V. Narayanan, *Eur. J. Med. Chem.*, **76**, 256 (2014); https://doi.org/10.1016/j.ejmech.2014.02.010
34. M.N. Cardoza-Contreras, A. Vasquez-Gallegos, A. Vidal-Limon, J.M. Romo-Herrera, S. Aguila and O.E. Contreras, *Catalysts*, **9**, 165 (2019); https://doi.org/10.3390/catal9020165

35. E. Pazos-Ortiz, J.H. Roque-Ruiz, E.A. Hinojos-Márquez, J. López-Esparza, A. Donohué-Cornejo, J.C. Cuevas-González, L.F. Espinosa-Cristóbal and S.Y. Reyes-López, *J. Nanomater.*, **2017**, 4752314 (2017); https://doi.org/10.1155/2017/4752314
36. N.A.R. Gow, J.P. Latge and C.A. Munro, *Microbiol. Spectr.*, **5**, FUNK-0035-2016 (2017); https://doi.org/10.1128/microbiolspec.FUNK-0035-2016
37. L.E. Cowen, D. Sanglard, S.J. Howard, P.D. Rogers and D.S. Perlin, *Cold Spring Harb. Perspect. Med.*, **5**, a019752 (2015); https://doi.org/10.1101/cshperspect.a019752
38. S. Soren, S. Kumar, S. Mishra, P.K. Jena, S.K. Verma and P. Parhi, *Microb. Pathog.*, **119**, 145 (2018); https://doi.org/10.1016/j.micpath.2018.03.048
39. R. Rajeswari and H.G. Prabu, *Process Biochem.*, **93**, 36 (2020); https://doi.org/10.1016/j.procbio.2020.03.010
40. S. Paul, J.P. Saikia, S.K. Samdarshi and B.K. Konwar, *J. Magn. Magn. Mater.*, **321**, 3621 (2009); https://doi.org/10.1016/j.jmmm.2009.07.004
41. R. Mandal, S. Ghosh, T. Mandal and P. Sahoo, *React. Chem. Eng.*, **8**, 143 (2023); https://doi.org/10.1002/slct.202203353
42. F.A. Alharthi, A.A. Alghamdi, N. Al-Zaqri, H.S. Alanazi, A.A. Alsyahi, A. El-Marghany and N. Ahmad, *Sci. Rep.*, **10**, 20229 (2020); https://doi.org/10.1038/s41598-020-77426-y
43. P. Panchal, D.R. Paul, A. Sharma, P. Choudhary, P. Meena and S.P. Nehra, *J. Colloid Interface Sci.*, **563**, 370 (2020); https://doi.org/10.1016/j.jcis.2019.12.079
44. M. Nandasana, T. Imboon, R. Layek, A. Dey, P. Pandya, V.S. Parihar, M.S. Tawre, S. Sutar, P. Kumbhakar, K. Pardesi, S. Thongmee and S. Ghosh, *Environ. Sci. Adv.*, **4**, 97 (2024); https://doi.org/10.1039/D4VA00295D
45. D. Thatikayala, V. Banothu, J. Kim, D.S. Shin, S. Vijayalakshmi and J. Park, *J. Mater. Sci. Mater. Electron.*, **31**, 5324 (2020); https://doi.org/10.1007/s10854-020-03093-4
46. H. Lim, M. Yusuf, S. Song, S. Park and K.H. Park, *RSC Adv.*, **11**, 8709 (2021); https://doi.org/10.1039/D0RA10945B
47. L. Bai, X. Zhang, Z. Ding, X. Wang and Y. Huang, *J. Taiwan Inst. Chem. Eng.*, **103**, 118 (2019); https://doi.org/10.1016/j.jtice.2019.08.002
48. E. Makauki, S.G. Mtavangu, O.D. Basu, M. Rwiza and R. Machunda, *Discov. Nano*, **18**, 142 (2023); https://doi.org/10.1186/s11671-023-03925-2
49. B.A. Fahimmunisha, R. Ishwarya, M.S. AlSalhi, S. Devanesan, M. Govindarajan and B. Vaseeharan, *J. Drug Deliv. Sci. Technol.*, **55**, 101465 (2020); https://doi.org/10.1016/j.jddst.2019.101465
50. N. Jomehzadeh, Z. Koolivand, E. Dahdouh, A. Akbari, A. Zahedi and N. Chamkouri, *Mater. Today Commun.*, **27**, 102457 (2021); https://doi.org/10.1016/j.mtcomm.2021.102457
51. M.C. Jobe, D.M.N. Mthiyane, M. Mwanza and D.C. Onwudiwe, *Heliyon*, **8**, e12243 (2022); https://doi.org/10.1016/j.heliyon.2022.es12243